Anisotropic filamentation instability of intense laser beams in plasmas near the critical density

Z.-M. Sheng, K. Nishihara, T. Honda,* Y. Sentoku, and K. Mima
Institute of Laser Engineering, Osaka University, Yamada-oka 2-6, Suita, Osaka 565-0871, Japan

S. V. Bulanov
General Physics Institute, Russian Academy of Science, Moscow 117942, Russia
(Received 14 June 2001; published 26 November 2001)

The relativistic filamentation instability (RFI) of linearly polarized intense laser beams in plasmas near the critical density is investigated. It is found that the RFI is anisotropic to transverse perturbations in this case; a homogeneous laser beam evolves to a stratified structure parallel to the laser polarization direction, as demonstrated recently with three-dimensional particle-in-cell simulations by Nishihara *et al.* [Proc. SPIE **3886**, 90 (2000)]. A weakly relativistic theory is developed for plasmas near the critical density. It shows that the anisotropy of the RFI results from a suppression of the instability in the laser polarization direction due to the electrostatic response. The anisotropic RFI is also analyzed based on an envelope equation for the laser beam. Finally, the envelope equation is solved numerically, and anisotropic filamentation and self-focusing are illustrated.

DOI: 10.1103/PhysRevE.64.066409 PACS number(s): 52.35.Mw, 52.38.−r, 52.65.−y

I. INTRODUCTION

The study of parametric instabilities of laser light in plasmas has attracted renewed interest owing to the advent of high-power lasers. Since such instabilities involve many physical processes such as anomalous absorption, fast electron generation, generation of high amplitude plasma waves, self-focusing and filamentation, etc., they are expected to play an important role in the context of fast ignition of fusion targets and other related applications. In earlier studies, attention was paid mainly to the case of tenuous plasma and moderate light intensities [1–7]. In recent years, theories have been developed to cover other parameter regimes including high plasma densities, relativistic light intensities, and relativistic plasma energies [8–12]. These theories are, however, valid only for circularly polarized (CP) laser light. The problem for linearly polarized (LP) laser light is more complicated owing to the presence of harmonic components in such laser irradiated plasmas [13]. However, currently high-power lasers are usually available with linear polarization.

Recently, parametric instabilities have been studied for LP lasers in homogeneous plasma—near and above critical density—using three-dimensional (3D) particle-in-cell (PIC) simulations [14]. One of the observed features, absent for CP lasers, is the anisotropic filamentation of laser light. The growth rate of the filamentation instability in the laser polarization direction is found to be much weaker than in the direction perpendicular to the polarization plane. An initially homogeneous laser beam evolves to a stratified structure parallel to the laser polarization, which can therefore be referred to as stratification instability. A theory is developed for plasma at the relativistic critical density (where the k vector of the laser light in plasma is zero) [14]. Related work was recently reported where parametric instabilities of LP lasers were discussed in a moving frame, where the k vector of the laser light is zero [15]. It should be pointed out that the anisotropic filamentation instability was noted nearly 30 years ago by Kaw *et al.*, who found that the growth rates of the filamentation instability caused by the ponderomotive force are different in directions along and perpendicular to the wave field [4]. Drake *et al.* have included contributions of both electromagnetic and electrostatic side band modes in their general dispersion relation of parametric instabilities [2]. At high plasma densities, electrostatic modes are predominant and anisotropic filamentation is expected. However, the relativistic nonlinearity, which is expected to be one of the dominant factors for the observed anisotropic filamentation instabilities in these 3D PIC simulations, was not included in those theoretical studies. We note that there were a few theoretical studies [16–21] as well as experimental observations [22–24] of relativistic self-focusing and filamentation instability. However, most of these studies are limited to cases with tenuous plasma densities, where relativistic self-focusing and filamentation instability are all transversely isotropic.

Motivated by the 3D PIC simulation results mentioned above, this paper is devoted to both analytical and numerical investigation of the filamentation instability caused by relativistic effects [relativistic filamentation instability (RFI)] in high plasma density regime. We show that the feature of the relativistic filamentation instability changes from isotropic in tenuous plasma to anisotropic in plasma near the critical density [25]. In Sec. II, parametric instabilities for a LP laser are studied analytically in the weakly relativistic approximation, by allowing perturbations with wave vectors in the laser polarization direction, an extension to the works by Max *et al.* [3] and McKinstrie and Bingham [7]. In particular, we show that the RFI growth rate is anisotropic to the transverse perturbations when the plasma is near the critical density, consistent with our 3D PIC simulation [14]. In very tenuous plasmas, isotropic filamentation is recovered. In Sec. III, the

*Present affiliation: Sony Corporation, Shinagawa, Tokyo 141-0001, Japan

RFI is studied with the envelope evolution equation. The anisotropic RFI growth rate is derived. The instability growth rates for modest plasma densities can be expressed in a similar way as those of Kaw *et al.* when cast in terms of a general dielectric function [4]. Section IV is devoted to numerical calculations based on the envelope equation, including electron density modulation. By using appropriate boundary conditions, both anisotropic filamentation instability and self-focusing are illustrated. In anisotropic self-focusing, an initially symmetric laser beam evolves to a elliptic beam elongated in the polarization direction. The paper concludes with a discussion in Sec. V.

II. ANISOTROPIC FILAMENTATION INSTABILITY AT WEAKLY RELATIVISTIC LIGHT INTENSITIES

In the weakly relativistic approximation, the following equations describe the coupling between laser fields and electron motion:

$$\nabla^2\mathbf{A}-\frac{1}{c^2}\frac{\partial^2\mathbf{A}}{\partial t^2}=\frac{1}{c}\frac{\partial}{\partial t}\nabla\phi+\frac{\omega_p^2}{c^2}n\mathbf{v}, \tag{1}$$

$$\frac{\partial\mathbf{v}}{\partial t}=\frac{\partial\mathbf{A}}{\partial t}+c\nabla\left(\phi-\frac{v^2}{2}\right)-\frac{1}{2}\frac{\partial}{\partial t}(v^2\mathbf{v}), \tag{2}$$

$$\frac{\partial n}{\partial t}+c\nabla\cdot(n\mathbf{v})=0, \tag{3}$$

$$\nabla^2\phi=\frac{\omega_p^2}{c^2}(n-1), \tag{4}$$

where $\mathbf{A}$ and ϕ are the vector and scalar potentials normalized by mc^2/e, $\mathbf{v}$ is the electron velocity normalized by c, n is the electron density normalized by the unperturbed density N_0, and $\omega_p^2=4\pi N_0e^2/m$ is the electron plasma frequency. In obtaining Eq. (1), the Coulomb gauge $\nabla\cdot\mathbf{A}=0$ has been used. For a LP laser field $\mathbf{A}_0=a_0\hat{\mathbf{y}}\cos(\theta_0)$, the density variation associated with the driving field can be written as $n_0=1+n_{02}\cos(2\theta_0)+\cdots$ and the velocity $\mathbf{v}_0=v_{01}\hat{\mathbf{y}}\cos(\theta_0)+v_{02}\hat{\mathbf{x}}\cos(2\theta_0)+\cdots$, where $\theta_0=k_0x-\omega_0t$, $\hat{\mathbf{x}}$ and $\hat{\mathbf{y}}$ are the unit vectors in the x and y directions, $v_{01}=a_0$, $v_{02}=[k_0c\omega_0/(4\omega_0^2-\omega_p^2)]a_0^2$, and $n_{02}=[k_0^2c^2/(4\omega_0^2-\omega_p^2)]a_0^2$. As a result, we have the dispersion relation [3]

$$\omega_0^2=k_0^2c^2+\omega_p^2\left[1-a_0^2\left(\frac{3}{8}-\frac{1}{2}\frac{k_0^2c^2}{4\omega_0^2-\omega_p^2}\right)\right]. \tag{5}$$

The perturbed equations of Eqs. (1)–(4) can be written as

$$\nabla^2\tilde{\mathbf{A}}-\frac{1}{c^2}\frac{\partial^2\tilde{\mathbf{A}}}{\partial t^2}=\frac{1}{c}\frac{\partial}{\partial t}\nabla\tilde{\phi}+\frac{\omega_p^2}{c^2}(n_0\tilde{\mathbf{v}}+\tilde{n}\mathbf{v}_0), \tag{6}$$

$$\frac{\partial\tilde{\mathbf{v}}}{\partial t}=\frac{\partial\tilde{\mathbf{A}}}{\partial t}+c\nabla\tilde{\phi}-c\nabla(\tilde{\mathbf{v}}\cdot\mathbf{v}_0)-\frac{1}{2}\frac{\partial}{\partial t}[v_0^2\tilde{\mathbf{v}}+2(\tilde{\mathbf{v}}\cdot\mathbf{v}_0)\mathbf{v}_0], \tag{7}$$

$$\frac{\partial\tilde{n}}{\partial t}=-c\nabla\cdot(n_0\tilde{\mathbf{v}}+\tilde{n}\mathbf{v}_0), \tag{8}$$

$$\nabla^2\tilde{\phi}=\frac{\omega_p^2}{c^2}\tilde{n}. \tag{9}$$

As usual, we expand $\tilde{\mathbf{A}}$, $\tilde{\mathbf{v}}$, $\tilde{n}$, and $\tilde{\phi}$ in the form of $\tilde{f}=\Sigma_{m=-\infty}^{+\infty}\tilde{f}_m\exp[i(\theta+m\theta_0)]$, with $\theta=\mathbf{k}\cdot\mathbf{x}-\omega t$, so that Eqs. (6)–(9) can be written as

$$D_m\tilde{\mathbf{A}}_m=c\omega_m\mathbf{k}_m\tilde{\phi}_m+\omega_p^2(\tilde{\mathbf{v}}_m+\mathbf{F}_m+\mathbf{G}_m), \tag{10}$$

$$\omega_m\tilde{\mathbf{v}}_m=\omega_m\tilde{\mathbf{A}}_m-c\mathbf{k}_m\tilde{\phi}_m+c\mathbf{k}_mH_m-\omega_m\mathbf{R}_m, \tag{11}$$

$$\omega_m\tilde{n}_m=c\mathbf{k}_m\cdot(\tilde{\mathbf{v}}_m+\mathbf{F}_m+\mathbf{G}_m), \tag{12}$$

$$k_m^2c^2\tilde{\phi}_m=-\omega_p^2\tilde{n}_m, \tag{13}$$

where $\omega_m=\omega+m\omega_0$, $\mathbf{k}_m=\mathbf{k}+mk_0\hat{\mathbf{x}}$, $D_m=\omega_m^2-c^2k_m^2$, $k_m=|\mathbf{k}_m|$, and

$$\mathbf{F}_m=\tfrac{1}{2}n_{02}(\tilde{\mathbf{v}}_{m+2}+\tilde{\mathbf{v}}_{m-2}),$$

$$\mathbf{G}_m=\tfrac{1}{2}a_0(\tilde{n}_{m+1}+\tilde{n}_{m-1})\hat{\mathbf{y}},$$

$$H_m=\tfrac{1}{2}a_0(\tilde{v}_{y,m+1}+\tilde{v}_{y,m-1}),$$

$$\mathbf{R}_m=\tfrac{1}{8}a_0^2(2\tilde{\mathbf{v}}_m+\tilde{\mathbf{v}}_{m+2}+\tilde{\mathbf{v}}_{m-2})+\tfrac{1}{4}a_0^2\times(2\tilde{v}_{y,m}+\tilde{v}_{y,m+2}+\tilde{v}_{y,m-2})\hat{\mathbf{y}},$$

where $\tilde{v}_{y,m}$ illustrates the y component of $\tilde{\mathbf{v}}_m$. Multiplying Eq. (11) by $\mathbf{k}_m$ and substituting $\mathbf{k}_m\cdot\tilde{\mathbf{v}}_m$ into Eq. (12), making use of Eq. (13) and $\mathbf{k}_m\cdot\tilde{\mathbf{A}}_m=0$ for the Coulomb gauge, we obtain the following expressions for the perturbation variables:

$$\mathbf{k}_m\cdot\tilde{\mathbf{v}}_m=D_{p,m}^{-1}[\omega_p^2\mathbf{k}_m\cdot(\mathbf{F}_m+\mathbf{G}_m)-\omega_m^2\mathbf{k}_m\cdot\mathbf{R}_m+c\omega_mk_m^2H_m],$$

$$\tilde{n}_m=D_{p,m}^{-1}[c\omega_m\mathbf{k}_m\cdot(\mathbf{F}_m+\mathbf{G}_m-\mathbf{R}_m)+c^2k_m^2H_m],$$

$$\tilde{\phi}_m=-(\omega_p^2/k_m^2c^2)D_{p,m}^{-1}[c\omega_m\mathbf{k}_m\cdot(\mathbf{F}_m+\mathbf{G}_m-\mathbf{R}_m)+c^2k_m^2H_m],$$

$$\tilde{\mathbf{v}}_m=\tilde{\mathbf{A}}_m-\mathbf{R}_m+\frac{\omega_p^2\mathbf{k}_m}{k_m^2D_{p,m}}\mathbf{k}_m\cdot(\mathbf{F}_m+\mathbf{G}_m-\mathbf{R}_m)+\frac{c\mathbf{k}_m\omega_m}{D_{p,m}}H_m.$$

where $D_{p,m}=\omega_m^2-\omega_p^2$. Note that the expressions for $\tilde{n}_m$ and $\tilde{\mathbf{v}}_m$ are recurrently related to each other through $\mathbf{F}_m$, $\mathbf{G}_m$, H_m, and $\mathbf{R}_m$. Substituting $\tilde{\mathbf{v}}_m$ and $\tilde{\phi}_m$ into Eq. (10), we obtain the equation for the vector potential:

$$D_m\tilde{\mathbf{A}}_m=\omega_p^2\left(1-\frac{\mathbf{k}_m\mathbf{k}_m}{k_m^2}\right)\cdot(\tilde{\mathbf{A}}_m+\mathbf{F}_m+\mathbf{G}_m-\mathbf{R}_m). \tag{14}$$

One can obtain a dispersion relation for the parametric instabilities from this equation. Here we note that the term proportional to $\mathbf{k}_m[\mathbf{k}_m\cdot(\tilde{\mathbf{A}}_m+\mathbf{F}_m+\mathbf{G}_m-\mathbf{R}_m)]$ was not included in earlier studies [3,7]. It is concerned with the electrostatic perturbation (in the polarization direction of the driving wave), and is responsible for the anisotropism of the filamentation instability. Generally, by use of Eqs. (6), (8), and (9), one finds that the right hand side $\mathcal{R}$ of Eq. (6) or (14) is equal to

$$\mathcal{R}=\omega_p^2\left(1-\frac{\mathbf{k}_m\mathbf{k}_m}{k_m^2}\right)\cdot(\widetilde{n\mathbf{v}})_m,$$

which is valid even without invoking the weakly relativistic approximation. Taking the component of the last equation in the polarization direction, one finds $\mathbf{k}_m[\mathbf{k}_m\cdot(\widetilde{n\mathbf{v}})_m]/k_m^2 \sim(\widetilde{nv_y})_m k_y^2/(k^2+m^2k_0^2)$, where k_y is the y component of $\mathbf{k}$ and $k=|\mathbf{k}|$. This has been identified in tenuous plasma and in dense plasma near the critical density, albeit general proof on its validity for arbitrary plasma density is still quested. In tenuous plasma with $\omega_p^2\ll\omega_0^2$ and $k\ll k_0$, the last term can be ignored compared to $(\widetilde{nv_y})_m$. One then finds that parametric instabilities are isotropic with respect to transverse perturbations. However, if $\omega_p^2\sim\omega_0^2$ and $k_0\ll k$, one finds parametric instabilities are anisotropic with respect to transverse perturbations.

For calculations up to order $O(a_0^2)$ in the weakly relativistic approximation with $a_0^2\ll 1$, it is enough to include $m=\pm 1$ for $\tilde{\mathbf{A}}_m$ and up to $m=\pm 2$ for $\tilde{\mathbf{v}}_m$ and $\tilde{n}_m$. Note that $\tilde{\mathbf{A}}_0$ is found to be of the order of $O(a_0^2\tilde{\mathbf{A}}_{\pm 1})$, and can be neglected, i.e., the low frequency mode is predominantly electrostatic. In this approximation, the density perturbation, as well as $\tilde{\mathbf{v}}_0$ and $\tilde{\mathbf{v}}_{\pm 2}$ are given by [to order $O(a_0\tilde{v})$]

$$\tilde{n}_0=\frac{c^2k^2}{2D_{p,0}}a_0(\tilde{v}_{y,1}+\tilde{v}_{y,-1}),$$

$$\tilde{n}_{\pm 1}=\frac{c^2k_{\pm 1}^2}{2D_{p,\pm 1}}a_0(\tilde{v}_{y,0}+\tilde{v}_{y,\pm 2}),$$

$$\tilde{n}_{\pm 2}=\frac{c^2k_{\pm 2}^2}{2D_{p,\pm 2}}a_0\tilde{v}_{y,\pm 1},$$

$$\tilde{\mathbf{v}}_0=\frac{c\omega\mathbf{k}}{2D_{p,0}}a_0(\tilde{v}_{y,1}+\tilde{v}_{y,-1}),$$

$$\tilde{\mathbf{v}}_{\pm 2}=\frac{c\omega_{\pm 2}\mathbf{k}_{\pm 2}}{2D_{p,\pm 2}}a_0\tilde{v}_{y,\pm 1},$$

and the y component of the right hand side of Eq. (14) is given by

$$S_{y,\pm 1}=\omega_p^2\left[1-a_0^2\left(\frac{3}{8}-\frac{1}{2}\frac{k_0^2c^2}{4\omega_0^2-\omega_p^2}\right)+g_\pm\right]\tilde{A}_{y,\pm 1}+\omega_p^2h_\pm\tilde{A}_{y,\mp 1}, \tag{15}$$

where $\tilde{A}_{y,\pm 1}$ is the y component of $\tilde{\mathbf{A}}_{\pm 1}$, and

$$g_\pm=\left[\frac{1}{4}\left(\frac{k^2c^2}{D_{p,0}}+\frac{k_{\pm 2}^2c^2}{D_{p,\pm 2}}\right)\left(1-\frac{k_y^2}{k_{\pm 1}^2}\right)-\frac{1}{2}\frac{k_0^2c^2}{4\omega_0^2-\omega_p^2}-\frac{3}{8}\left(1-\frac{4k_y^2}{3k_{\pm 1}^2}\right)\right]a_0^2,$$

$$h_\pm=\left[\frac{1}{4}\frac{k^2c^2}{D_{p,0}}\left(1-\frac{k_y^2}{k_{\pm 1}^2}\right)+\frac{1}{2}\frac{k_0^2c^2}{4\omega_0^2-\omega_p^2}-\frac{3}{8}\left(1-\frac{2k_y^2}{3k_{\pm 1}^2}\right)\right]a_0^2.$$

In deriving Eq. (15), we have substituted $\tilde{v}_{y,\pm 1}$ with $\tilde{A}_{y,\pm 1}$ to keep terms up to $O(a_0^2\tilde{A}_{y,\pm 1})$ only in this equation. We mention that, rather than generally, Eq. (15) has been derived particularly for tenuous plasma and for dense plasma near the critical density. A general expression valid for arbitrary plasma density is still not available. We will therefore limit ourselves to these two particular cases in the following studies in this section. Using the coupled equations for $\tilde{A}_{y,\pm 1}$ from Eqs. (14) and (15) and the dispersion relation for the driving wave [Eq. (5)], we obtain the dispersion relation for the perturbed wave,

$$(\tilde{D}_+-\omega_p^2g_+)(\tilde{D}_--\omega_p^2g_-)=\omega_p^4h_+h_-, \tag{16}$$

where $\tilde{D}_\pm=\omega^2-c^2k^2\pm 2(\omega\omega_0-\mathbf{k}\cdot\mathbf{k}_0c^2)$. In the case of low plasma density, $\omega_p\ll\omega_0$, $\omega\ll\omega_0$, and $k_y\ll k\ll k_0$, $k_{\pm m}\approx m^2k_0^2$, we recover the well-known dispersion relation [3,7], which describes Raman forward and backward scattering, relativistic self-modulation, and filamentation instability in tenuous plasma.

In the following, we are interested mainly in the pure filamentation instability with $\mathbf{k}\cdot\mathbf{k}_0=0$. In this case, the dispersion relation can be simplified to

$$\omega^2=\frac{k^2c^2}{4\omega_0^2}[k^2c^2+(g_++g_-)\omega_p^2] \tag{17}$$

assuming $\omega\ll kc$, where $k=(k_y^2+k_z^2)^{1/2}$ and $k_x=0$. At a low plasma density, one finds $g_\pm\approx[-3/4+k_0^2c^2/(4\omega_0^2-\omega_p^2)]a_0^2/2$, since $(1-k_y^2/k_0^2)\approx 1$ and assuming $\omega^2\ll\omega_p^2$ and $k^2c^2\ll\omega_p^2$. It shows that the RFI growth rate in the y direction is the same as in the z-direction, i.e. the filamentation is isotropic in this case. The maximum growth rate is [3] $\Gamma_{max}=(\omega_p^2/4\omega_0)a_0^2q$ when $k^2c^2=a_0^2q\omega_p^2/2$, consistent with previous assumptions for ω^2 and k^2c^2. Here $q=3/4-k_0^2c^2/(4\omega_0^2-\omega_p^2)\sim 1/2$.

For the case of near critical plasma density $\omega_p\sim\omega_0$, we have $k_0\ll k$ and $k_{\pm 1}^2\approx k^2$. We again assume that $\omega^2\ll\omega_p^2$ and $c^2k^2\ll\omega_p^2$, so that $g_\pm\approx-[\frac{3}{8}(1-4k_y^2/3k^2)]a_0^2$. For a given k, the instability growth rate is a function of k_y/k. If the perturbation is only in the laser polarization (y) direction,

i.e., $k_z=0$ and $k=k_y$, it is obvious that there is no instability since $g_{\pm}=a_0^2/8$, and we always have $\omega^2>0$. On the other hand, if the perturbation is only in the z direction, i.e., $k_y=0$ and $k=k_z$, we have $g_{\pm}=-(3/8)a_0^2$ and there is instability for $c^2k_z^2<(3/4)a_0^2\omega_p^2$. The maximum instability growth rate is found to be $\Gamma_{max}=(3/16)a_0^2\omega_p^2/\omega_0$ when $k_z^2c^2=(3/8)a_0^2\omega_p^2$, consistent with previous assumptions for ω^2 and k^2c^2. Therefore, the filamentation instability develops in the direction perpendicular to the laser polarization, although it is suppressed in the direction of laser polarization. This anisotropic property of the RFI growth rate with respect to transverse wave numbers of the perturbation is in agreement with that observed in 3D PIC simulations [14]. In addition, in plasmas near the critical density, since $k_0\approx 0$ and the group velocity reduces to zero, perturbations in the x direction are almost the same as in the z direction, i.e., relativistic modulational instability (RMI) becomes equivalent to RFI in this case. This is also found in 3D PIC simulations [14]. One can verify this as well by calculating the RMI growth rate from Eq. (16).

III. FILAMENTATION INSTABILITY ANALYSIS WITH THE ENVELOPE EQUATION

One can also analyze the anisotropic RFI with the envelope equation obtained from the slowly varying envelope approximation. In the weakly relativistic approximation, Eqs. (1)–(4) lead to

$$\frac{1}{c^2}\frac{\partial^2\mathbf{A}}{\partial t^2}-\nabla^2\mathbf{A}=\frac{i\omega_0}{c}\boldsymbol{\epsilon}\nabla\phi-\frac{\omega_0^2}{c^2}(1-\epsilon)\mathbf{A}, \tag{18}$$

$$\nabla\cdot(\boldsymbol{\epsilon}\nabla\phi)=i\frac{\omega_0}{c}\nabla\boldsymbol{\epsilon}\cdot\mathbf{A}, \tag{19}$$

where

$$\epsilon=1-(\omega_p^2/\omega_0^2)n\left[1-|a^2|\left(\frac{3}{8}-\frac{1}{2}\frac{k_0^2c^2}{4\omega_0^2-\omega_p^2}\right)\right],$$

n is the slowly varying electron density normalized to the unperturbed density, and a is the amplitude of the electron quiver velocity at the fundamental frequency. Equation (19) describes the response of plasma to the laser field owing to inhomogeneity in plasma density and/or laser intensity, which is just the well-known relation $\nabla\cdot\mathbf{E}=-\boldsymbol{\epsilon}^{-1}\nabla\boldsymbol{\epsilon}\cdot\mathbf{E}$. Here the electric field $\mathbf{E}=i\mathbf{A}-(c/\omega_0)\nabla\phi$, which is normalized by $m\omega_0c/e$. Equations (18) and (19) are equivalent to [26,27]

$$\frac{1}{c^2}\frac{\partial^2\mathbf{E}}{\partial t^2}-\nabla^2\mathbf{E}-\nabla(\boldsymbol{\epsilon}^{-1}\nabla\boldsymbol{\epsilon}\cdot\mathbf{E})=-\frac{\omega_0^2}{c^2}(1-\epsilon)\mathbf{E}. \tag{20}$$

We now study the RFI by use of the envelope evolution equation. Let $\mathbf{A}=\frac{1}{2}\hat{\mathbf{y}}a(t,x,y,z)\exp(ik_0x-i\omega_0t)+\text{c.c.}$ and $\phi=\frac{1}{2}\varphi(t,x,y,z)\exp(ik_0x-i\omega_0t)+\text{c.c.}$, where a and φ vary slowly as compared to $\exp(-i\omega_0t)$, and $\hat{\mathbf{y}}$ is the unit vector in the y direction. Assuming that $|\partial a/\partial t|\ll|\omega_0 a|$, from Eqs. (18) and (19) we obtain

$$2i\frac{\omega_0}{c^2}\frac{\partial a}{\partial t}+2ik_0\frac{\partial a}{\partial x}+\nabla^2a+i\frac{\omega_0}{c}\boldsymbol{\epsilon}\frac{\partial\varphi}{\partial y}+\left(\frac{\omega_0^2}{c^2}\boldsymbol{\epsilon}-k_0^2\right)a=0, \tag{21}$$

$$\nabla\boldsymbol{\epsilon}\cdot(\nabla+ik_0\hat{\mathbf{x}})\varphi+\boldsymbol{\epsilon}\left(\nabla^2+2ik_0\frac{\partial}{\partial x}-k_0^2\right)\varphi=i\frac{\omega_0}{c}\frac{\partial\boldsymbol{\epsilon}}{\partial y}a, \tag{22}$$

where $\nabla^2=\partial^2/\partial x^2+\nabla_\perp^2$ and $\nabla_\perp^2=\partial^2/\partial y^2+\partial^2/\partial z^2$, and $\hat{\mathbf{x}}$ is the unit vector point to the x direction. Note that we have not invoked the paraxial approximation by keeping the term of a second order derivative with respective to x (i.e., $\partial^2/\partial x^2$) [28], since it is in the same order of magnitude as $\nabla_\perp^2$ when the plasma density is close to the critical density [29]. Then, assuming that the unperturbed wave amplitude is homogeneous in space and time, we perform a perturbation analysis following Zakharov [30]. Let $a=A\exp(i\psi)$ and $\varphi=\varphi_1\exp(i\psi)$, with $A=a_0+a_1\exp(i\mathbf{k}\cdot\mathbf{x}-i\omega t)$ and $\psi=\psi_0+\psi_1\exp(i\mathbf{k}\cdot\mathbf{x}-i\omega t)$, where a_0 is a constant independent of time and space; ψ_0 is independent of space, but can be dependent on time, and $\mathbf{k}=k_x\hat{\mathbf{x}}+k_y\hat{\mathbf{y}}+k_z\hat{\mathbf{z}}$ is the wave number of transverse perturbations. We find the relativistic filamentation and modulational instability growth rate

$$\Gamma=\frac{c^2}{2\omega_0}k\left[\frac{2\omega_0^2}{c^2}\left(a_0^2\frac{d\epsilon_0}{da_0^2}\right)\left(1-\frac{k_y^2}{k_\perp^2+(k_0+k_x)^2}\right)-k^2\right]^{1/2}, \tag{23}$$

where $k_\perp=(k_y^2+k_z^2)^{1/2}$, $k=(k_\perp^2+k_x^2)^{1/2}$, and $\boldsymbol{\epsilon}_0=\boldsymbol{\epsilon}|_{a=a_0}$. For the modulation instability in the longitudinal direction, the real frequency is given by $\omega=k_0k_xc^2/\omega_0$, as found in other ways [3]. For the pure filamentation instability when $k_x=0$, the RFI shown by Eq. (23) illustrates an anisotropic feature similar to that described by Eq. (17) given in Sec. II. Note that some small corrections in Eq. (17) are caused by higher side bands, which cannot be taken into account starting with envelope equations. In very tenuous plasma with $k_0=\epsilon_0^{1/2}\omega_0/c\approx\omega_0/c\gg k_\perp$, a weakly anisotropic effect is found. From Eq. (23), the maximum growth rate for a perturbation in the z direction is found to be $\Gamma_{max}=\omega_0a_0^2\epsilon_0'/2$ when $k_z^2=(\omega_0^2/c^2)a_0^2\epsilon_0'$, where $\epsilon_0'=d\epsilon_0/da_0^2\propto\omega_p^2/\omega_0^2$. Similarly, the maximum growth rate for a perturbation in the y direction is $\Gamma_{max}=\omega_0a_0^2\epsilon_0'(1+2a_0^2\epsilon_0'/\epsilon_0)^{-1/2}/2$ when $k_y^2=(\omega_0^2/c^2)a_0^2\epsilon_0'(1+2a_0^2\epsilon_0'/\epsilon_0)^{-1}$. Note that these expressions are essentially identical to those of Kaw *et al.* [4], who described the instability in terms of spatial growth rates. In dense plasma near the critical density with $k_0\approx 0$, the anisotropic effect is strong. In this case, if there is a transverse perturbation perpendicular to the polarization (i.e., $k_y=0$ and $k_z\neq 0$), we obtain the normal filamentation instability; whereas if the perturbation is along the polarization direction (i.e., $k_y\neq 0$ and $k_z=0$), there is no filamentation instability.

Also in this case, Eq. (23) shows that the relativistic modulational instability in the x direction is almost equivalent to the RFI in the z direction.

In deriving this instability growth rate, we only account for the nonlinearity owing to the relativistic effect, i.e., nonlinearity due to density modification is not considered by setting $n=1$ in ϵ_0. This limitation is removed in the numerical calculation given in next Sec. III. In the weakly relativistic approximation, using the dielectric constant given above, we have

$$\frac{d\epsilon_0}{da_0^2}=\frac{\omega_p^2}{\omega_0^2}\left(\frac{3}{8}-\frac{1}{2}\frac{k_0^2c^2}{4\omega_0^2-\omega_p^2}\right).$$

Generally, however, it is is difficult to express the dielectric constant at an arbitrary intensity for linearly polarized light in plasma. In some limited parameter regime, it was shown that $\epsilon_0=1-a_0^{-1}(\pi^2/8)(\omega_p^2/\omega_0^2)$ when $a_0\gg 1$ and $1/\epsilon_0\gg 1$ [31–34]. In many cases, it can be approximated by [27] $\epsilon_0=1-(\omega_p^2/\omega_0^2)/\gamma_0$ with $\gamma_0=(1+a_0^2/2)^{1/2}$. In this case, one has

$$\frac{d\epsilon_0}{da_0^2}=\frac{\omega_p^2}{\omega_0^2}\frac{1}{4\gamma_0^3}.$$

Figure 1(a) shows the RFI growth rate, obtained with Eq. (23), and the last expression for $d\epsilon_0/da_0^2$, as a function of $\theta=\tan^{-1}(k_y/k_\perp)$, for varying plasma densities. At a low plasma density, the RFI growth rate is isotropic. With an increase of the plasma density, the RFI in the y direction is reduced both in growth rate and k-vector space, as shown in Fig. 1(b). Close to the critical plasma density $\omega_p^2/\omega_0^2=\gamma_0$, the instability for perturbations in the y direction is completely suppressed. Note that the magnitude of the instability growth rate ($\Gamma/\omega_0<0.1$) indicates that the approximation $|\partial a/\partial t|\ll|\omega_0 a|$ used above is applicable.

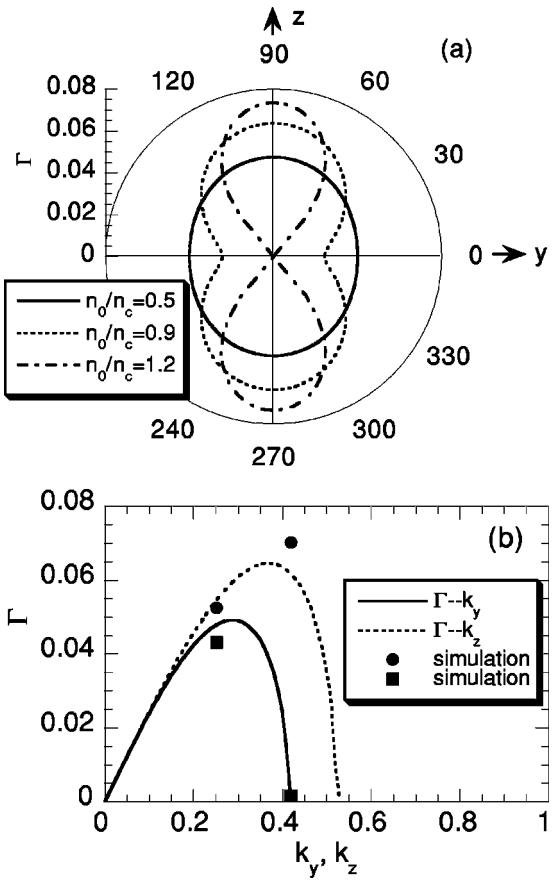

FIG. 1. (a) RFI growth rate (normalized by ω_0^{-1}) as a function of angular direction $\theta=\tan^{-1}(k_y/k_\perp)$ for $a_0=1$, $k_\perp=0.4\omega_p/c$, and $k_x=0$ at various densities. (b) RFI growth rate as a function of wave numbers of transverse perturbations (normalized by ω_p/c) for $a_0=1$ and $n_0/n_c=0.9$. The filled squares and dots are obtained from numerical simulations for $n_0/n_c=0.9$ for perturbations in the y and z directions, respectively.

IV. NUMERICAL RESULTS

In the numerical calculations, we solve Eq. (20) instead of solving the coupled equations (18) and (19). In the slowly varying envelope approximation, assuming $\mathbf{E}=\frac{1}{2}\hat{\mathbf{y}}a_e(t,x,y,z)\exp(ik_0x-i\omega_0t)+\text{c.c.}$ and $|\partial a_e/\partial t|\ll|\omega_0 a_e|$, Eq. (20) can be reduced to

$$2i\left(\frac{\partial}{\partial\tau}+\frac{k_0c}{\omega_p}\frac{\partial}{\partial x}\right)a_e+\frac{\partial^2a_e}{\partial x^2}+\nabla_\perp^2a_e+\frac{\partial}{\partial y}\left(a_e\frac{\partial\ln\epsilon}{\partial y}\right)+(1-n/\gamma)a_e=0, \tag{24}$$

where a_e is the complex amplitude of the electric field; $\tau=\omega_p^2t/\omega_0$; coordinates x, y, and z are normalized by c/ω_p; and $\epsilon=1-(\omega_p^2/\omega_0^2)(1+i\nu/\omega_0)^{-1}n/\gamma$, with $\gamma=(1+|a_e|^2/2)^{1/2}$. Here a free parameter ν, allowing for collisional absorption, is introduced to avoid possible vanishing ϵ, since we shall deal with plasma near a critical density. It is clear in Eq. (24) that the term $(\partial/\partial y)[a_e\partial\ln\epsilon/\partial y]$ causes a transversely anisotropic RFI. The numerical calculation is conducted with the coordinate transform from (τ,x,y,z) to (τ,ξ,y,z) with $\xi=x-(k_0c/\omega_p)\tau$. In this case, the first three terms on the left hand side of Eq. (24) are reduced to $(2i\partial/\partial\tau+\partial^2/\partial\xi^2)a_e$. Thus, within this mathematical transformation, the ξ coordinate is equivalent to the z coordinate, both of which are perpendicular to the laser polarization direction. If the plasma is at the critical density (or $k_0=0$), the ξ (or x) and z coordinates are exactly equivalent [14]. Under this consideration, we only keep one of these two coordinates, say the z coordinate, in the following numerical calculation. This corresponds to neglecting the longitudinal beam profile and suppressing the longitudinal perturbation. Thus the resulting equation is

$$2i\frac{\partial a_e}{\partial\tau}+\nabla_\perp^2a_e+\frac{\partial}{\partial y}\left(a_e\frac{\partial\ln\epsilon}{\partial y}\right)+(1-n/\gamma)a_e=0. \tag{25}$$

Although obtained under a different physical consideration, this appears in the same form as derived within the paraxial approximation. In the numerical solution, the electron den-

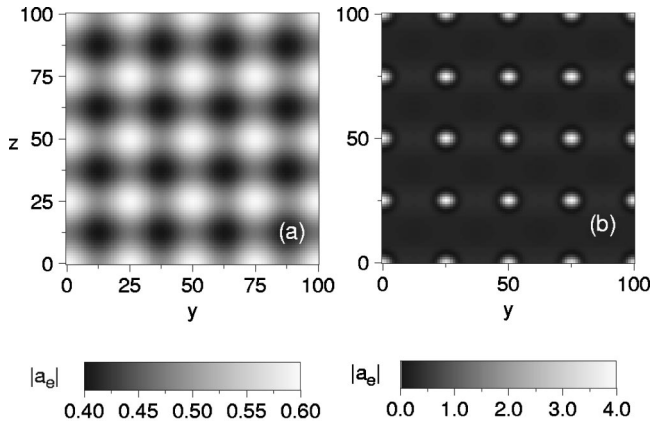

FIG. 2. Snapshots of the amplitude distribution in transverse space for $a_0=0.5$, $n_0/n_c=0.5$, $\delta a=0.005$, and $k_y=k_z=8\pi/100$ at (a) $\tau=100$ and (b) $\tau=180$.

sity is now allowed to change with time, and is given by $n=Max(0,1+\nabla_\perp^2\gamma)$ or its modified version [16] $n=1+\nabla_\perp^2(\gamma+\alpha\ln n)$, where $\alpha=T_e/mc^2$. Note that without the transversely anisotropic term $(\partial/\partial y)[a_e\partial\ln\epsilon/\partial y]$, Eq. (25) is the same evolution equation that is used to study self-focusing in tenuous plasma [16–22].

Equation (25) is solved with the algorithm of the alternating-direction implicit method [35]. A rectangular simulation box is used in the *y*-*z* plane, and the amplitude $a_e(\tau,y,z)$ is represented as a set of values $a_e|_{i,j}^n$ defined at time step $n\Delta\tau$ and space coordinates $(i\Delta y, j\Delta z)$, where $\Delta\tau$ is the time step of integration, Δy and Δz are the mesh size in y and z directions, $i=0,1,\ldots,I-1$ and $j=0,1,\ldots,J-1$.

A periodic boundary condition is used to simulate the anisotropic filamentation instability, where $a_e|_{i=0,j}^n=a_e|_{i=I,j}^n$ and $a_e|_{i,j=0}^n=a_e|_{i,j=J}^n$. The initial transverse profile of the laser beam amplitude is set to be $a_e=a_0+\delta a[\cos(k_y y)+\cos(k_z z)]$, which represents a perturbation (with amplitude δa) both in y and z directions superimposed on a homogeneous distribution (of amplitude a_0). In the following simulation, we typically take $\delta a=0.005$. The initial perturbation amplitude only affects the code-running time to grow to a certain level; it does not change the physical results. On the other hand, other parameters such as a_0, k_y, k_z, and ω_p^2/ω_0^2 $(=n_0/n_c)$ are relevant to the final results. Figure 2 shows snapshots of the amplitude profile for $a_0=0.5$ and $n_0/n_c=0.5$. It is found that the initial homogeneous distribution evolves into separated filaments, each with a maximum amplitude over 3. The filament spots are elliptically elongated in the laser polarization (y) direction. Figure 3 illustrates the simulation results for $n_0/n_c=0.9$. In contrast to the previous case, the filamentation instability develops much faster in the z direction than in the y direction, and the initially homogeneous distribution evolves to a stratified structure parallel to the laser polarization direction. Detailed time evolution of the filamentation process is displayed for this example in Figs. 3(c)–3(f). The above examples support the theory proposed in Secs. II and III that the RFI is anisotropic in the transverse perturbation when the plasma density is near the

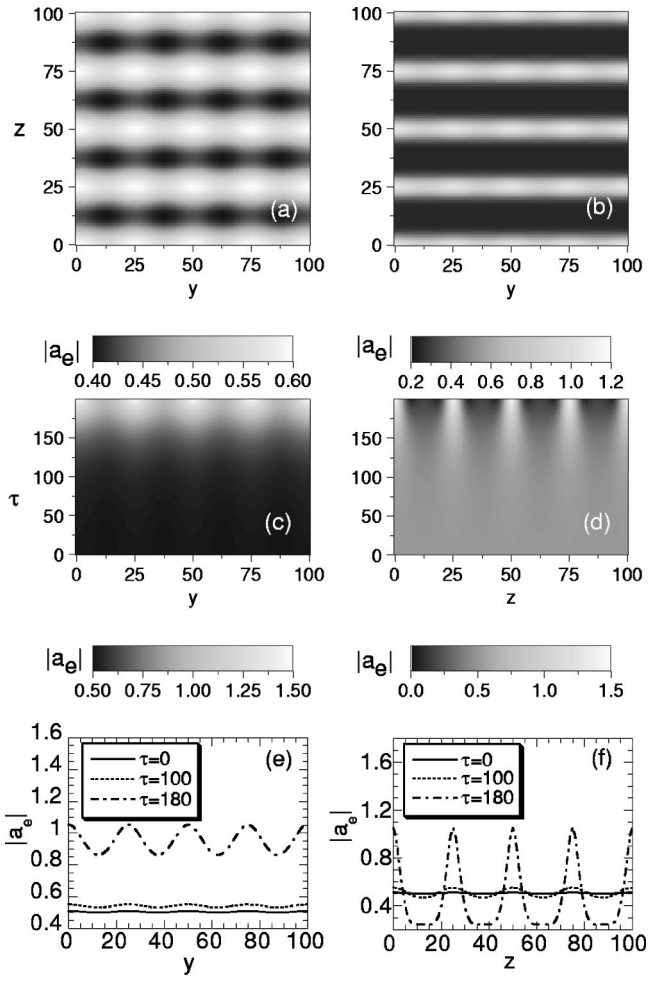

FIG. 3. Amplitude distribution in transverse space for $a_0=0.5$, $n_0/n_c=0.9$, and $k_y=k_z=8\pi/100$. (a) Snapshot at $\tau=100$. (b) Snapshot at $\tau=180$. (c) Time-space plot in the y direction cut at $z=50$. (d) Time-space plot in the z direction cut at $y=50$. (e) Snapshots in the y direction cut at $z=50$. (f) Snapshots in the z direction cut at $y=50$.

critical density. In three-dimensional geometry, since the dependence of the laser amplitude on the x coordinate is similar to the z coordinate in this case, one expects that the laser beam develops into many light stripes along the polarization direction. Actually, this has been observed in 3D PIC simulations [14].

In the case of a higher laser intensity, anisotropic filamentation occurs at higher density. Figures 4(a) and 4(b) show the cases when $a_0=1$ and $n_0/n_c=0.5$ and 0.9, respectively. Compared with Fig. 3 for the same densities, one finds that the anisotropic effect is stronger at lower intensity. This is because, with higher intensity, the effective plasma density is reduced due to the relativistic effect. Figures 4(c) and 4(d) demonstrate that the anisotropic effect will occur in overdense plasma if the laser intensity is high enough to relativistically induce transparency.

In PIC simulations and in actual experiments, the filamentation instability is determined mainly by the the perturbation modes corresponding to the maximum growth rate, since many modes are present at the same time due to noise. In the

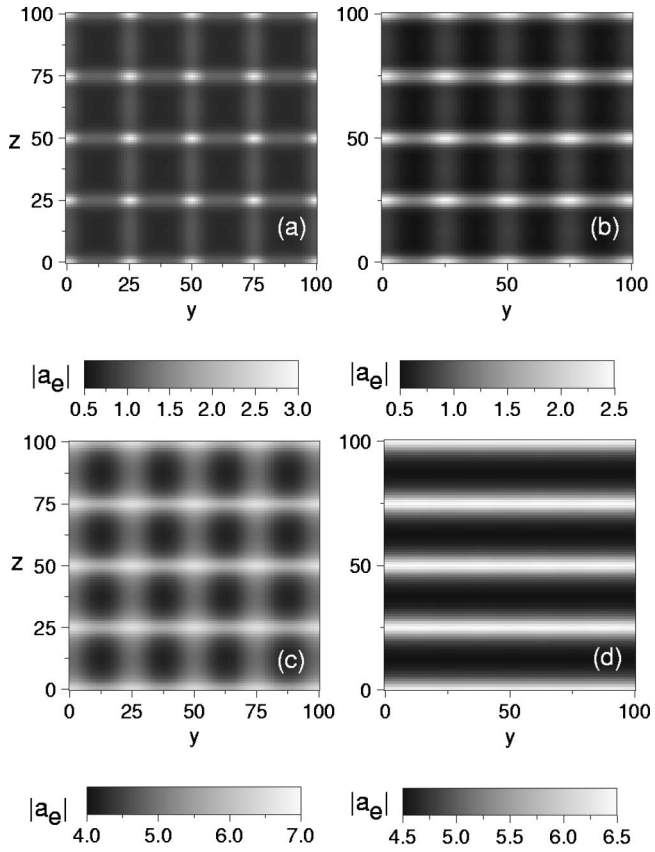

FIG. 4. Snapshots of the amplitude distribution in transverse space. Frames (a) and (b) are for $a_0=1.0$, and $k_y=k_z=8\pi/100$ at $\tau=80$ for $n_0/n_c=0.5$ and 0.9, respectively. Frames (c) and (d) are for $a_0=5.0$ and $k_y=k_z=8\pi/100$ at $\tau=90$ for $n_0/n_c=1.5$ and 3.0, respectively.

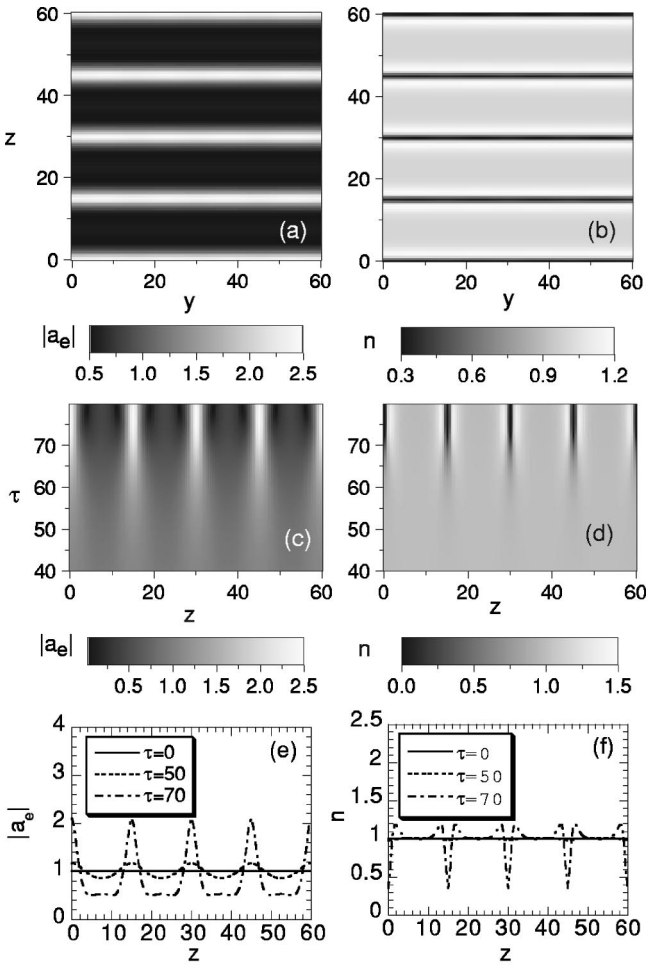

FIG. 5. Amplitude and electron density distributions in transverse space for $a_0=1.0$, $n_0/n_c=0.9$, and $k_y=k_z=8\pi/60$. (a) Snapshot of amplitude at $\tau=70$. (b) Snapshot of electron density at $\tau=70$. (c) Time-space plot of the amplitude in the z direction cut at $y=30$. (d) Time-space plot of the electron density in the z direction cut at $y=30$. (e) Snapshots of the amplitude in the z direction cut at $y=30$. (f) Snapshots of the electron density in the z direction cut at $y=30$.

present simulation of the evolution equation, perturbations are input as initial conditions, allowing one to study the development of the filamentation instability for given perturbation wave numbers. In Fig. 5, we plot snapshots of the amplitude profile for $a_0=1$ and $n_0/n_c=0.9$ at an increased perturbation wave number $k_y=k_z=8\pi/60$. Compared with Fig. 4(b), a stronger anisotropic effect is observed in this case. It reveals that the anisotropy of the RFI depends not only on the plasma density but also on perturbation wave numbers. The calculated instability growth rate is in agreement with analytical theory, as shown in Fig. 1(b). Figures 5(c) and 5(d) illustrate the time evolution of the filamentation. It is found that after a certain time, sharply peaked amplitude and density distributions are produced, as shown in Figs. 5(e) and 5(f). Around $\tau=75$, these peaks break, and a collapselike instability occurs [36,37]. We find that this numerical collapselike instability is directly connected to the occurrence of a vanishing dielectric constant ϵ in some regions, which results in a sudden increase in the field amplitude. By introducing collisional damping in the dielectric constant, this instability can be removed for large enough ν (~ 0.05 in this case). A similar behavior is also found for a laser beam with a finite transverse size, as discussed in the following.

We point out that the field energy can be changed gradually even before the occurrence of collapselike instability. According to the envelope equation (24), for either periodic boundary conditions or boundary conditions such that $|a_e|$ vanishes for infinite $|y|$ or $|z|$, one finds that

$$\frac{dP}{d\tau}=-\frac{i}{2}\int\frac{\partial\ln\epsilon}{\partial y}\left(a_e\frac{\partial a_e^*}{\partial y}-a_e^*\frac{\partial a_e}{\partial y}\right)dydz,$$

where $P=\int|a_e|^2dydz$; a_e^* is the complex conjugate of a_e. This shows that the transverse field energy is usually not conserved due to the anisotropic term. This is not surprising, since a_e includes electrostatic fields in addition to the laser field, implying an energy exchange with electrons during the evolution. Moreover, one may note that the energy contained in the longitudinal field is not accounted for in P. This field, pointing in the laser propagation direction, coexists with the transverse field when $\partial a_e/\partial y\neq 0$. The transverse field energy is conserved only when $\partial a_e/\partial y=0$ everywhere, i.e.,

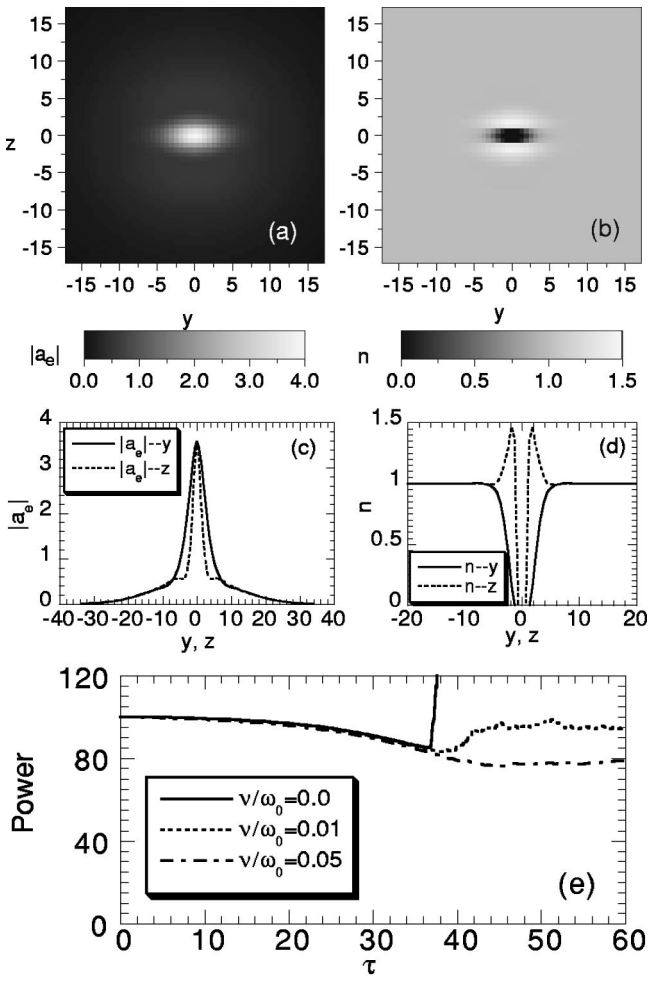

FIG. 6. Evolution of amplitude and electron density when the laser beam is transversely in a Gaussian profile initially with $a_0=1.0$, $n_0/n_c=0.9$, and $\rho_0=10.0$. Frames (a) and (b) are snapshots of the amplitude and electron density, respectively, at $\tau=35$. Frames (c) and (d) show the y and z profiles of the amplitude and electron density as cut at $z=0$ and $y=0$, respectively, at $\tau=35$. Frame (e) is the time evolution of the beam power for different ν.

there is no longitudinal field and no electrostatic field excitation by the transverse electric field component in the laser polarization direction. Usually, the total transverse field energy decreases when the transverse size of filaments or beam decreases, and vice versa.

Let us now simulate the self-focusing of laser beams, with boundary conditions such that $|a_e|$ vanishes as $|y|$ or $|z|$ goes to infinity. An initially Gaussian beam profile is used: $a_e=a_0\exp[-(y^2+z^2)/2\rho_0^2]$, which is cylindrically symmetric. The normalized threshold power for self-focusing is about $P=\int a_e^2\rho d\rho\geqslant 8$, i.e., $a_0^2\rho_0^2\geqslant 16$ according to Refs. [17,38,39]. Figure 6 shows snapshots of the amplitude profile and electron density for initial $a_0=1.0$, $n_0/n_c=0.9$, and $\rho_0=10.0c/\omega_p$. The cylindrically symmetric beam evolves into an elliptic structure elongated in the laser polarization direction. Meanwhile, the corresponding electron density profile is also anisotropic, and electron cavitation appears in a much reduced space. Normally, the higher the background plasma density, the larger the ellipticity of the beam spot. In this example, collapselike instability is also observed after $\tau=35$ if $\nu=0$, leading to an unphysical result, e.g., the irregular structure of the amplitude profile and the sharp increase in the amplitude and energy, as shown in Fig. 6(e). Although beam collapse is possible in a medium with cubic nonlinearity [36,37], there is no beam collapse for symmetric self-focusing in plasma because the effect of electron cavitation removes the nonlinearity inside the beam core. As a result, stable self-focusing of laser beams in plasma is possible even if its power is many times the critical power [16]. In the present case, we find that the collapselike instability is numerically connected with a vanishing dielectric constant in some region. Similar to the case of a homogeneous beam discussed previously, the singularity in the vanishing dielectric constant can be removed by introducing a finite collisional frequency, as shown by the time evolution of the power in Fig. 6(e). On the other hand, since strong mode-conversion and particle acceleration are expected after the occurrence of a vanishing dielectric constant and collapselike instability, our model would not be valid beyond this stage, even if we introduce a collisional frequency. Finally, if the plasma density is much less than the critical density, symmetric self-focusing is reproduced whenever the beam power is above the self-focusing threshold, and no collapselike instability is observed, as expected.

V. CONCLUSIONS AND DISCUSSIONS

The relativistic filamentation instability (RFI) has been studied both analytically and numerically. We show that the electrostatic response of electrons in the laser polarization (y) direction tends to prevent the growth of a perturbation in this direction for plasma densities near the critical density. However, a RFI in the z direction can develop with the same growth rate as the relativistic modulation instability (in the propagation x direction), if the effective plasma density n_0/γ_0 is close to the critical density. As a result, a homogeneous laser beam will evolve into a stratified structure parallel to the laser polarization. For the same reason, a cylindrically symmetric laser beam will evolve into an elliptic form in the beam cross section elongated in the laser polarization direction. The analytical theory is in agreement with the numerical calculations based on the envelope equation and with our recent 3D PIC simulation results [14].

Our model for the numerical calculation is based on the envelope equation, which can be reduced to a paraboliclike equation. The equation has been solved only for the transverse section of the laser beam, which excludes the coupling with the longitudinal modulation instability. This is one of the main limitations of the present model. Future work could be devoted to directly solving Eq. (24) in three-dimensional space or even Eq. (20) as done in Ref. [40], though without invoking the cylindrical symmetry for the transverse beam section.

Our model does not include magnetic field generation re-

sulting from a laser driven current of fast electrons and the Weibel instability. Their effects on the laser filamentation instability are not yet clear. However, since 3D simulations show a robust anisotropic filamentation with all the factors included, it is expected that the effects of magnetic field and fast electrons are only of peripheral importance to the anisotropic filamentation instability, at least in the early stage. The anisotropic filamentation instability and self-focusing of laser beams could result in anisotropic angular distributions of fast electrons and corresponding bremsstrahlung emission. Since the anisotropy is very strong at a high plasma density, it could be looked for in future experiments.

ACKNOWLEDGMENTS

Z.M.S. was supported by the Japan Society for the Promotion of Science. He wishes to thank Professor T. Yamaka for his encouragement and support. He is also grateful to Professor Wei Yu for stimulating discussions. We thank Visiting Professor A. Offenberger for carefully reading the manuscript and improving the text.

[1] W.L. Kruer, *The Physics of Laser Plasma Interaction* (Addison-Wesley, New York, 1988).
[2] J.F. Drake, P.K. Kaw, Y.C. Lee, G. Schmidt, C.S. Liu, and M. Rosenbluth, Phys. Fluids **17**, 778 (1974).
[3] C.E. Max, J. Arons, and A.B. Langdon, Phys. Rev. Lett. **33**, 209 (1974).
[4] P.K. Kaw, G. Schmidt, and T. Wilcox, Phys. Fluids **16**, 1522 (1973).
[5] D.W. Forslund, J.M. Kindel, and E. Lindman, Phys. Fluids **18**, 1002 (1975).
[6] K. Estabrook and W.L. Kruer, Phys. Fluids **26**, 1892 (1983).
[7] C.J. Mckinstrie and R. Bingham, Phys. Fluids B **4**, 2626 (1992).
[8] S. Guerin, G. Laval, P. Mora, J.C. Adam, A. Heron, and A. Bendib, Phys. Plasmas **2**, 2807 (1995).
[9] C.D. Decker, W.B. Mori, K.-C. Tzeng, and T. Katsouleas, Phys. Plasmas **3**, 2047 (1996).
[10] A.S. Sakharov and V.I. Kirsanov, Plasma Phys. Rep. **21**, 596 (1995); **21**, 587 (1995).
[11] B. Quesnel, P. Mora, J.C. Adam, A. Heron, and G. Laval, Phys. Plasmas **4**, 3358 (1997); B. Quesnel, P. Mora, J.C. Adam, S. Guerin, A. Heron, and G. Laval, Phys. Rev. Lett. **78**, 2132 (1997).
[12] Z.M. Sheng, K. Mima, Y. Sentoku, and K. Nishihara, Phys. Rev. E **61**, 4362 (2000).
[13] H.C. Barr, S.J. Berwick, and P. Mason, Phys. Rev. Lett. **81**, 2910 (1998).
[14] K. Nishihara, T. Honda, S.V. Bulanov, and Z.M. Sheng, Proc. SPIE **3886**, 90 (2000); T. Honda, K. Nishihara, T. Okamoto, S. Bulanov, Z.M. Sheng, M. Okamoto, and Y. Fukuda, J. Plasma Fusion Res. **75**, 219 (1999).
[15] H.C. Barr, P. Mason, and D.M. Parr, Phys. Rev. Lett. **83**, 1606 (1999); Phys. Plasmas **7**, 2604 (2000).
[16] M.D. Feit, A.M. Komashko, S.L. Musher, A.M. Rubenchik, and S.K. Turitsyn, Phys. Rev. E **57**, 7122 (1998).
[17] G.Z. Sun, E. Ott, Y.C. Lee, and P. Guzdar, Phys. Fluids **30**, 526 (1987).
[18] A.B. Borisov, A.V. Borovski, O.B. Shiryaev, V.V. Korobkin, A.M. Prokhorv, J.C. Solem, T.S. Luk, K. Boyer, and C.K. Rhodes, Phys. Rev. A **45**, 5830 (1992).
[19] X.L. Chen and R.N. Sudan, Phys. Fluids B **5**, 1336 (1993).
[20] Z.M. Sheng and J. Meyer-ter-Vehn, Phys. Rev. E **54**, 1833 (1996).
[21] F. Vidal and T.W. Johnston, Phys. Rev. Lett. **77**, 1282 (1996).
[22] R. Fedosejevs, X.F. Wang, and G.D. Tsakiris, Phys. Rev. E **56**, 4615 (1997).
[23] P. E. Young, in *Atomic Processes in Plasmas*, edited by Albert L. Osterherd and William Hi Goldstein, AIP Conf. Proc. No. 381 (AIP, Woodbury, NY, 1996).
[24] R. Wagner, S.-Y. Chen, A. Maksimchuk, and D. Umstadter, Phys. Rev. Lett. **78**, 3125 (1997).
[25] Z. M Sheng, K. Nishihara, T. Honda, K. Mima, and S. Bulanov, in *Inertial Fusion Sciences and Applications'99*, edited by C. Labaune, W. J. Hogan, and K. A. Tanaka (Elsevier, Paris, 2000), p. 376.
[26] T. Hänser, W. Scheid, and H. Hora, J. Opt. Soc. Am. B **5**, 2029 (1988).
[27] H.S. Brandi, C. Manus, G. Mainfray, T. Lehner, and G. Bonnaud, Phys. Fluids B **5**, 3539 (1993).
[28] M.D. Feit and J.A. Fleck, Jr., J. Opt. Soc. Am. B **5**, 633 (1988).
[29] H.A. Rose and D.F. DuBois, Phys. Fluids B **5**, 3337 (1993).
[30] V.E. Zakharov, Zh. Éksp. Teor. Fiz. **53**, 1735 (1967) [Sov. Phys. JETP **26**, 994 (1968)].
[31] A.I. Akhiezer and P.V. Polovin, Zh. Éksp. Teor. Fiz. **30**, 915 (1956) [Sov. Phys. JETP **3**, 696 (1956)].
[32] P. Kaw and J. Dawson, Phys. Fluids **13**, 472 (1970).
[33] C. Max and E. Perkins, Phys. Rev. Lett. **27**, 1342 (1971).
[34] W.B. Mori, C.D. Decker, and W.P. Leemans, IEEE Trans. Plasma Sci. **21**, 110 (1993).
[35] W.H. Press, S.A. Teukolsky, W.T. Vetterling, and B.P. Flannery, *Numerical Recipes in Fortran* (Cambridge University Press, New York, 1992), p. 861.
[36] V.E. Zakharov, V.V. Sobolev, and V.C. Synakh, Zh. Éksp. Teor. Fiz. **60**, 136 (1971) [Sov. Phys. JETP **33**, 77 (1971)]; **62**, 1745 (1972) [**35**, 908 (1972)].
[37] J. Denavit, N.R. Pereira, and R.N. Sudan, Phys. Rev. Lett. **33**, 1435 (1974).
[38] P. Sprangle, C.M. Tang, and E. Esarey, IEEE Trans. Plasma Sci. **PS-15**, 145 (1983).
[39] G. Schmidt and W. Horton, Comments Plasma Phys. Controlled Fusion **9**, 85 (1985).
[40] G. Bonnaud, H.S. Brandi, C. Manus, G. Mainfray, and T. Lehner, Phys. Plasmas **1**, 968 (1994).